Tomography via Correlation of Noisy Measurement Records

Colm A. Ryan, Blake R. Johnson, Jay M. Gambetta, Jerry M. Chow, Marcus P. da Silva, Oliver E. Dial, and Thomas A. Ohki Raytheon BBN Technologies, Cambridge, MA 02138, USA IBM T.J. Watson Research Center, Yorktown Heights, NY 10598, USA (Dated: December 23, 2013)

We present methods and results of shot-by-shot correlation of noisy measurements to extract entangled state and process tomography in a superconducting qubit architecture. We show that averaging continuous values, rather than counting discrete thresholded values, is a valid tomographic strategy and is in fact the better choice in the low signal-to-noise regime. We show that the effort to measure N-body correlations from individual measurements scales exponentially with N, but with sufficient signal-to-noise the approach remains viable for few-body correlations. We provide a new protocol to optimally account for the transient behavior of pulsed measurements. Despite single-shot measurement fidelity that is less than perfect, we demonstrate appropriate processing to extract and verify entangled states and processes.

By engineering coherent manipulation of quantum states we hope to gain computational power not available to classical computers. The purported advantage of a quantum information processing system comes from its ability to create and control quantum correlations or entanglement [1]. As we work towards obtaining high-fidelity quantum control, the ability to measure, confirm and benchmark quantum correlations is an important tool for debugging and verification.

Measurement results for only parts of a system by themselves are insufficient to reconstruct the overall state of the system, or of a process acting on the system. These sub-system statistics cannot capture correlations, whether classical or quantum. Joint quantum measurements, ones that indicate the joint quantum state of a system, can provide information about the entire system, and thus allow for complete reconstruction of states or processes. These joint measurements may be intrinsically available or they may be effectively enabled by post-measurement correlation of the single-qubit results.

The physics of particular systems may enable such intrinsic joint measurements—for example, in a circuit quantum electrodynamics (QED) setup, the frequency shift of a resonator coupled dispersively to multiple qubits provides information about the joint state of the qubits [2, 3], or in an ion-trap system the total fluoresence from a chain of ions provides similar joint information [4]. However, there is a limit to the correlations that can be engineered while maintaining individual addressability and control. Alternatively, entangling operations between qubits, before their individual measurement, can implement effective joint measurements by mapping a multi-body observable to a single-qubit one [5], but these operations can also be error-prone or difficult to implement. Instead, an accessible approach to joint measurements is to measure individual qubits and *correlate* the separate single-shot records. This approach is common to other solid state qubits [6, 7], optical photonics [8] and microwave optics [9, 10].

When constructing joint measurements from correlating individual ones, one must address the requirements for the individual measurements in order to obtain high-fidelity reconstruction of multi-qubit states and processes. In particular, since errors in the individual measurements will propagate into correlations, one might wonder if low-fidelity individual measurements make it difficult or impossible to reconstruct entangled states. Fortunately, circuit QED allows for high-visibility measurements even when the single-shot fidelity is poor [11], meaning that the dominant measurement noise is state-independent. This allows for a strategy that is not available with traditional counting detectors: correlate the continuous measurement response without thresholding into binary outcomes. We will show that averaging such continuous outcomes allows for an unbiased estimate of multi-qubit observables, and is the best strategy in the low signal-to-noise (SNR) regime.

Whenever correlating noisy individual measurements, there is reduced SNR in the correlated measurements. We will show that for N-body correlations this SNR penalty is generally exponential in N, but that in the large SNR regime reduces to 1/N. This implies that a greater amount of averaging is necessary to obtain accurate estimates of multi-body terms than single-body ones, but for the SNR available in current experiments, few-body correlations remain readily accessible.

Certain quantum computing architectures, such as the surface code [12], require individual qubit measurements which must be correlated for debugging and validation purposes. In a subsection of a circuit QED implementation of such an architecture, we present a phase-stable heterodyne measurement technique and a new filter protocol to optimize the SNR of a pulsed measurement. Using these techniques we verified that our measurements have a highly single-qubit character. Finally, we demonstrate the viability of correlating noisy measurement records by characterizing two-qubit states and entangling processes.

SOFT-AVERAGING VS. THRESHOLDING

Measurement in a circuit QED setup typically consists of coupling the qubit to an auxiliary meter (usually a cavity mode), and then inferring the qubit state from directly measuring the auxiliary mode. Since the qubit-mode coupling is effectively diagonal in the qubit's eigenbasis, the qubit POVMs corresponding to different measurement outcomes will always be diagonal as well, even when the measurement is not projective (i.e., when there is a finite probability of error for the measurement to distinguish between excited and ground states). Although the measurement of the meter can in principle take an unbounded continum of values, discrete outcomes can be obtained by thresholding to bin those measurement outcomes into a finite set. However, for tomography we are more interested in estimating the expectation value of observables than in the single-shot distinguishability of states. In this case, soft-averaging of the measurement records over many shots, without thresholding, can yield significant advantages.

A simple model of circuit QED measurement illustrates this quite vividly. In the absence of relaxation, measurements of the meter will yield a weighted mixture of Gaussian distributions. Each of these Gaussian distributions will have a mean and variance determined by details of the device, and the weights correspond to the probabilities of the qubit being in different eigenstates. In other words, conditioned on the qubit being prepared in an eigenstate i, the distribution of measurement outcomes is $N(\mu_i, \nu_i^2)$, where μ_i is the measurement eigenvalue. Soft-averaging over R shots scales the variance of the distributions by a factor of $\frac{1}{R}$, but an estimate of any diagonal observable will have an unbiased mean. Thresholding, on the other hand, will result in biased estimates of the expectation value because for Gaussian distributions there is always a finite probability of mistaking one measurement outcome for another. This bias can be corrected by rescaling the measurement results which converts the bias into additional variance. Soft-averaging also requires scaling to translate from measurement eigenvalues to the ± 1 outcomes expected for a Pauli operator measurement [13]. The mean-squared error (MSE), equal to the sum of the variance and the square of the bias, is a figure of merit one can use to evaluate how well we can estimate an observable. If we assume the bias can be correted then the best strategy is determined by the relative variance of the two approaches which will depend on the SNR of the individual measurements and the number of averages. In the low SNR regime soft-averaging is preferred whereas in the high SNR regime thresholding is better.

As a simple concrete example, consider the measurement of a single qubit, where $\nu_0 = \nu_1 = \nu$ and $\mu_0 = -\mu_1 = 1$. For an arbitrary state, soft-averaged estimates of $\langle \sigma_z \rangle$ will be distributed according to $N(\langle \sigma_z \rangle, \frac{\nu^2}{R} + \frac{1 - \langle \sigma_z \rangle^2}{R})$,

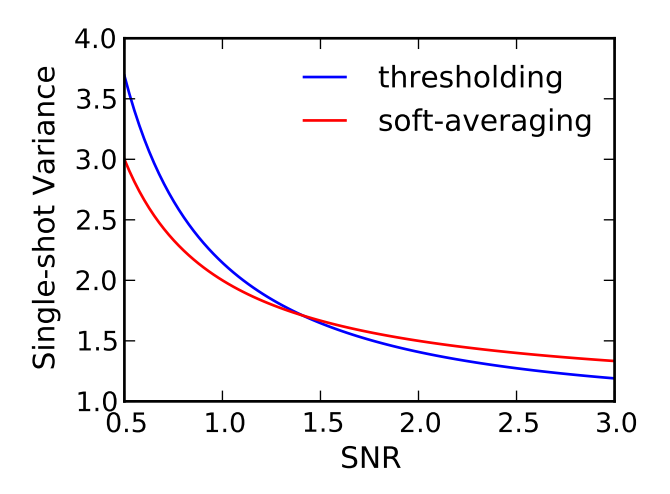


FIG. 1. The variance of soft-averaging and thresholding as a function of measurement SNR for a superposition state $(\langle \sigma_z \rangle = 0)$. At low SNR soft-averaging is the better choice but at high SNR it pays an extra penalty from the widths of the distributions whereas thresholding is only affected by the exponentially small overlap of the two Gaussians.

where the first variance term is the instrinic Gaussian variance and the second is quantum shot noise. Setting the threshold at zero, the thresholded estimates will have a mean given by $\langle \sigma_z \rangle [2\Phi(1/\nu\sqrt{2})-1]$, where Φ is the cumulative distribution function of a normal random variable, and variance of $\frac{1}{R} - \frac{\langle \sigma_z \rangle^2}{R} [2\Phi(1/\nu\sqrt{2})-1]^2$. Consequently, thresholding will introduce a bias of $2\langle \sigma_z \rangle [1-\Phi(1/\nu\sqrt{2})]$, which is independent of the number of averages, R. If we now assume we have perfect knowledge of the bias from calibration experiments then the rescaled thresholded variance is

$$\frac{1}{R[2\Phi(1/\nu\sqrt{2})-1]^2} - \frac{\langle \sigma_z \rangle^2}{R},\tag{1}$$

whereas it has not changed for soft-averaging. The SNR = $1/\nu^2$ where the variances are equal occurs at

$$\frac{1}{[2\Phi(1/\nu\sqrt{2}) - 1]^2} = \nu^2 + 1,\tag{2}$$

which is satisfied at SNR ≈ 1.41 (corresponding to a single-shot fidelity of 76%) and is unchanged as one correlates multiple measurements. Above this cross-over, soft-averaging pays an additional variance penalty which is exponentially worse than thresholding; however, as seen in Figure 1, in this regime we are often limited by quantum shot noise. Substantial advances in measurement fidelity in superconducting circuits due to the use of quantum-limited amplifiers[14–16], implies that the community will shortly enter the regime where thresholding is the preferred strategy.

SNR SCALING OF CORRELATION TERMS

There is a cost associated with using the correlations of subsystem measurements instead of joint measurements, which can be most easily illustrated by seeing how the accuracy of measurement estimates scales with the variance of the observations [17]. Consider a product state such that the measurement records X_i are independent random variables with mean and variance $(\langle \sigma_{z,i} \rangle, \nu_i^2 + (1 - \langle \sigma_{z,i} \rangle^2))$. Then the variance of the correlated records of N subsystems is given by [18],

$$\nu_{\text{corr}}^{2} = \text{Var}(X_{i_{1}}X_{i_{2}}\cdots X_{i_{N}})
= \Pi_{k=1}^{N}(\nu_{k}^{2} + (1 - \langle \sigma_{z,i} \rangle^{2}) + \langle \sigma_{z,i} \rangle^{2}) - \Pi_{k=1}^{N} \langle \sigma_{z,i} \rangle^{2}
= \left[\Pi_{k=1}^{N} (\nu_{k}^{2} + 1) - \langle \sigma_{z,1} \cdots \sigma_{z,N} \rangle^{2} \right].$$
(3)

 $\langle X_{i_1}X_{i_2}\cdots X_{i_N}\rangle^2$ is an unbiased estimate for $\langle \sigma_{z,1}\cdots \sigma_{z,N}\rangle^2$ so the MSE is equal to $\nu_{\rm corr}^2$ and it grows exponentially with the number of correlated terms. Entangled states will have correlated shot noise and the variance calculation is considerably more involved. However, for tomography of arbitrary states we are limited by this exponential scaling. It is possible to reduce the variance by repeating the measurement R times and averaging, but in order to get some fixed accuracy on the estimate of $\langle X_{i_1}X_{i_2}\cdots X_{i_N}\rangle$, R will still have to scale exponentially with N.

For small N, and equal and sufficiently high SNR ($\nu_k^2 = 1/\text{SNR} \ll 1$), then Eq. 3 reduces to,

$$\nu_{\rm corr}^2 \approx \frac{N}{\rm SNR},$$
 (4)

so R is simply linearly related to N in this favorable regime. Thus, measurements of low-weight correlators are still accessible without a punative experimental effort.

EXPERIMENTAL SETUP

Samples were fabricated with three single-junction transmon qubits in linear configuration with nearest-neighbours joined by bus resonators [19]. For the experiments discussed here, we used two of the three qubits, so the relevant subsystem is as shown in Fig. 2(b). Similar chips were measured at IBM and BBN. Each qubit has an individual measurement resonator coupled to it via the standard circuit QED Hamiltonian [20]. The same resonator is also used for driving the qubit dynamics with microwave pulses. The resonant frequency of the cavity exhibits a qubit-state dependence which we measure by the response of a microwave pulse applied near the cavity frequency.

We employed an "autodyne" approach, similar to Ref. [21] and shown in Fig. 2(a), to measure the qubit state via the reflection of a microwave pulse off the coupled cavity.

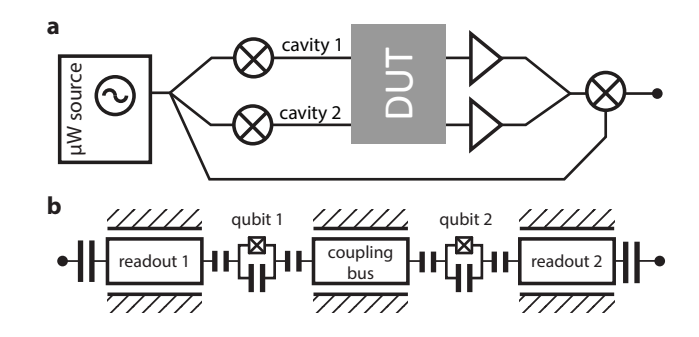


FIG. 2. (a) Schematic for a parsimonious two channel autodyne measurment. A single microwave source is split and both channels are SSB I/Q modulated to produce a shaped pulse at the cavity frequency. The refected signal is then amplified and mixed back down with an LO from the same microwave source. (b) Schematic of the two-qubit system with individual readout resonators and an unconnected coupling bus resonator.

Autodyning produces a heterodyne signal from a single local oscillator (LO). The microwave LO, detuned from the cavity, is single-sideband (SSB) modulated via an IQ mixer to bring the microwave pulse on-resonance with the cavity. The reflected amplified signal is then mixed down with the same microwave carrier. This eliminates the need for two microwave sources, nulls out any microwave phase drifts and moves the measurement away from DC. If the SSB modulation comes from an arbitrary waveform generator (AWG) it also allows for measurement pulse shaping. In addition, if multiple read-out cavities are close in frequency, it allows us to use a single microwave source to drive multiple channels with relatively less expensive power splitters and amplifiers.

At the readout side, the ability to choose the heterodyne IF frequency allows multiple readout channels to be frequency muliplexed onto the same high-speed digitizer and then digitally separated using techniques from software defined radio. Although our current implementation is purely in software, we expect it to readily transfer to hardware as we scale up the number of readout channels [22]. The initial data stream is sampled at 500MS/s and is immediately decimated with a low-pass finite-impulse response (FIR) filter. This allows us to achieve good phase precision with the relatively low vertical resolution (8-bits) of our digitizer card (AlazarTech 9870). The channels are then extracted with a frequency shifting low-pass filter. The bandwidth needed per channel is $(2\chi + \kappa)/2\pi$, where κ is the cavity linewidth, and χ the dispersive shift. For current parameters, this gives channels bandwidths of a few MHz. Future devices optimized for high-fidelity readout will have larger χ and κ , increasing the channel bandwidth to $\approx 10\,\mathrm{MHz}$. This is much smaller than the typical analog bandwidth of commercial digitizing hardware, allowing many readout signals to be multiplexed onto a single physical channel.

MEASUREMENT TOMOGRAPHY

Before analyzing correlated sub-system measurements, it helps to first optimize each individual readout and reduce the signal to a single quadrature. In the absence of experimental bandwidth constraints, elegant solutions to the optimal measurement filter exist [23]. However, when the measurement is made through a cavity, the measurement response is similar to that of a kicked oscillator [24] producing a phase transient in the response. During the rising edge of the pulse the reflected signal's phase swings wildly. Unfortunately, this is exactly the most crucial time in the record because it has been least affected by T_1 decay. Simple integration over a quadrature will lose information as the different phases cancel out. Here we use the mean ground and excited state traces as a matched filter [25] to unroll the measurement traces and weight them according to the time-varying SNR. The matched filter is optimal for SNR, which would also be optimal for measurement fidelity in the absence of T_1 . For the experiments considered here, T_1 is much greater than the cavity rise time, $1/\kappa$. In this case, the filter is close to the optimal linear filter.

To derive the matched filter consider that the measurement signal is given by

$$\psi(t) \propto \frac{1}{2} [\alpha_0(t) - \alpha_1(t)] \sigma_z + \xi(t), \tag{5}$$

where $\alpha_i(t)$ is the time-dependent cavity response when the qubit is in state i, and $\xi(t)$ is a zero-mean noise term that is uncorrelated with the state. The filtered measurement is given by an integration kernel, K(t), such that

$$S = \int_0^t K(t)\psi(t) \, \mathrm{d}t,\tag{6}$$

$$=\sum_{j}^{3}K_{j}\psi_{j},\tag{7}$$

where in the second form we discretize time such that $K_j = K(t_j)$ and $\psi_j = \psi(t_j)$. From this we can see that

$$\langle \Delta S \rangle = \sum_{j} K_{j} \langle \alpha_{0}(t_{j}) - \alpha_{1}(t_{j}) \rangle,$$
 (8)

$$\nu^2 = \operatorname{var}(\Delta S) = \sum_j K_j^2 \nu_j^2, \tag{9}$$

where $\langle \Delta S \rangle$ is the average difference of S for $\sigma_z = \pm 1$ and $\nu_j^2 = \text{var}(\alpha_0(t_j) - \alpha_1(t_j)) + \text{var}(\xi)$. Then, to optimize the SNR we set $\frac{\partial}{\partial K_j} \left| \langle S \rangle \right|^2 / \nu^2 = 0$. After dropping scaling factors that are independent of j, we find

$$K_{j} = \frac{D^{*}(t_{j})}{\nu_{j}^{2}},\tag{10}$$

where $D(t_j) = \langle \alpha_0(t_j) - \alpha_1(t_j) \rangle$ is the difference vector between the mean ground-state and excited-state responses. Since T_1 prevents fixing σ_z , we do not have direct

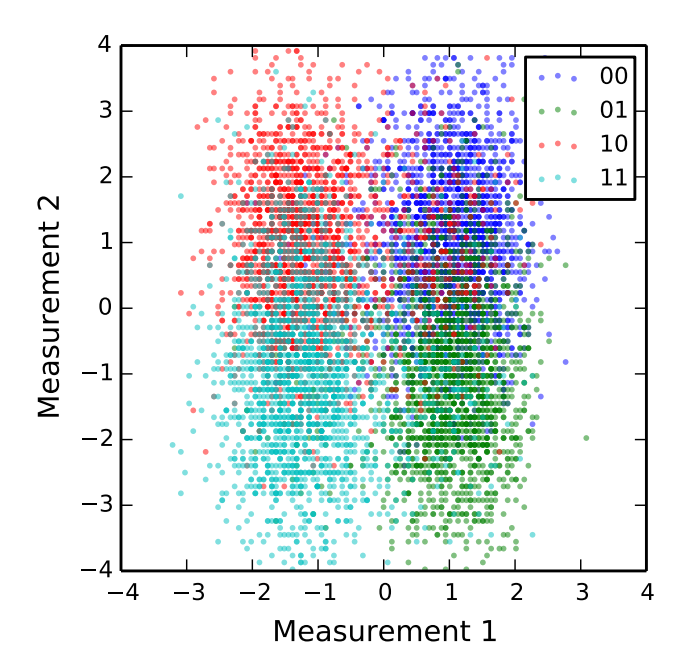


FIG. 3. Scatter of the filtered measurement results for both readout channels after preparation of the basis states $|00\rangle$ (blue), $|01\rangle$ (green), $|10\rangle$ (red), and $|11\rangle$ (cyan). Qubit 2 has a smaller effective coupling to its readout cavity, leading to increased variance along the measurement 2 axis.

access to D(t). Consequently, we approximate it by measuring the mean cavity response after preparing the qubit in σ_z basis states. Note that $\angle D$ gives the time-dependent quadrature containing qubit-state information. Thus, the above construction rotates all information into the real part of the resulting signal, so one can discard the orthogonal imaginary quadrature. We additionally subtract the mean response to remove the identity component in the measurement. This ensures that the resulting correlators are composed mostly of multi-body terms. Finally, the optimal integration time is determined by maximizing the single-shot fidelity.

In the tight confines of the chip there is inevitable microwave coupling between nominally independent lines that may inadvertently enable spurious multi-qubit readout. Therefore, it is important to confirm that the measurements give mostly independent single-qubit information and that our joint readout is enabled only from post-measurement correlation of the results. After verifying a sufficient level of qubit control with randomized benchmarking [26] we run a limited tomography on the measurement operators. By analyzing the measurements associated with preparing the four basis states, shown in Fig. 3, we can convert to expectation values of diagonal Pauli operators [2] and confirm limited multi-Hamming

State	00>	$ 01\rangle$	$ 10\rangle$	$ 11\rangle$
$M_1 \nu^2$	0.42	0.44	0.85	0.77
$M_2 \nu^2$	1.36	1.67	1.37	1.84
$\nu_{ m corr}^2$	2.35	2.85	3.39	4.02

TABLE I. Variances of M_1 and M_2 measurement operators and correlation variance for various computational-basis states. Variance increases when the corresponding qubit is prepared in the $|1\rangle$ (excited) state, due to increased variance from relaxation events (T_1) during measurement. The corresponding single-shot readout fidelities are 0.59 and 0.18, respectively.

weight operators.

$$\hat{M}_1 = 1.0110(4)ZI + 0.0164(6)IZ - 0.0106(6)ZZ$$

$$\hat{M}_2 = 0.00(1)ZI + 0.98(1)IZ + 0.02(1)ZZ$$

$$\hat{M}_{1,2} = 0.00(2)ZI + 0.00(2)IZ + 0.98(2)ZZ.$$
(11)

Given access to the single-shot measurement records, it is possible to estimate the variances associated with the different computational-basis states of each subsystem, and thus quantify the scaling of the correlated SNR. In the experiments discussed here, the subsystem measurement records have the single-shot variances shown in Table. I. The corresponding SNR's approach the cross-over between soft-averaging and thresholding. While a hybrid strategy could be envisaged, for simplicity we soft-average all results. Then, the correlations computed using (3) have variance ν_{corr}^2 between 2.35 and 4.02 for the different computational basis states. Thus, in order to resolve the correlated measurement $\langle \sigma_{z,1} \sigma_{z,2} \rangle$ to the same accuracy as $\langle \sigma_{z,1} \rangle$ we need ≈ 5 times more averaging.

TOMOGRAPHIC INVERSION

Tomographic inversion is the process of converting a set of measurements into a physical density matrix or process map. Since the estimates of single- and multi-body terms may have unequal variances, the standard inversion procedure should be modified to take these into account. The method below provides an estimator for states and processes that may be readily fed into a semidefinite program solver, if one wishes to add additional physical constraints (such as positivity in the process map) [27].

The correlated measurement records result in estimates of the expectation value $\langle \hat{M}_{(i,j,\cdots)} \rangle$ for the N-body observable

$$\hat{M}_{(i,j,\cdots)} = \hat{U}_i^{\dagger} \hat{M}_0 \hat{U}_i \otimes \hat{U}_i^{\dagger} \hat{M}_1 \hat{U}_j \otimes \cdots . \tag{12}$$

If the state $\hat{\rho}$ of the system is initially unknown, the problem of estimating $\hat{\rho}$ from a linearly-independent and informationally complete set of observables $\hat{M}_{(i,j,\cdots)}$ can be cast as a standard linear regression problem. Similarly,

if the system evolves according to some unknown superoperator \mathcal{E} , this superoperator can be estimated via linear regression by preparing various known initial states $\hat{\rho}_{\alpha}$ and measuring a linearly-independent and informationally complete set of observables $\hat{M}_{(i,j,\cdots)}$.

The best linear unbiased estimator for the reconstruction of a state or process can be computed exactly for the cases where the covariance matrix of the observations is known a priori—this corresponds to generalized least-squares (GLS) regression. In the quantum case, however, this covariance matrix depends on the state or process being reconstructed, and so it is never known a priori—the best linear unbiased estimator cannot be constructed. However, it can be approximated by empirically computing the covariance matrix of the observations. In the experiments described here, only the diagonal elements of the covariance matrix were computed and used in the reconstruction of the state or process, which leads to a slight bias in the estimate, although the mean squared-error performance is still good.

Formally, we can describe the state-tomography experiments as follows. Let $\text{vec}(\hat{A})$ be the column-major vectorization of an operator \hat{A} . Then the vector of state measurement expectation values m_s is given by

$$m_s = P_s \operatorname{vec}(\hat{\rho}),$$
 (13)

where

$$P_{s} = \begin{bmatrix} \operatorname{vec}(\hat{M}_{(0,0,\cdots,0,0)})^{\dagger} \\ \operatorname{vec}(\hat{M}_{(0,0,\cdots,0,1)})^{\dagger} \\ \vdots \end{bmatrix}, \tag{14}$$

is the state predictor matrix, relating the state $\hat{\rho}$ to the vector m_s of expectation values. Then, if we have an estimate \tilde{m}_s for the expectation values, an estimator for $\hat{\rho}$ is given by

$$\tilde{\rho} = P_s^+ \tilde{m}_s \tag{15}$$

where

$$P_s^+ = (P_s^{\dagger} C^{-1} P_s)^{-1} P_s^{\dagger} C^{-1}, \tag{16}$$

is the GLS equivalent of the Moore-Penrose pseudo-inverse of the state predictor, and where C is the empirical covariance for the measurements. In practice there are equivalent alternatives to computing $\tilde{\rho}$ explicitly that have better numerical stability properties.

Process-tomography experiments have an analogous description. The main distinction is that the predictor then maps a pair of input state and measurement observable to expectation values, so the vector of expectation values m_p is given by

$$m_p = P_p \text{vec}(\mathcal{E}),$$
 (17)

where \mathcal{E} is the Liouville representation [28] of the process being characterized, and the process tomography predictor matrix P_p is given by

$$P_{p} = \begin{bmatrix} \operatorname{vec}(\operatorname{vec}(\hat{M}_{(0,0,\cdots,0,0)})^{\dagger} \operatorname{vec}(\hat{\rho}_{(0,0,\cdots,0,0)}))^{\dagger} \\ \operatorname{vec}(\operatorname{vec}(\hat{M}_{(0,0,\cdots,0,1)})^{\dagger} \operatorname{vec}(\hat{\rho}_{(0,0,\cdots,0,0)}))^{\dagger} \\ \vdots \\ \operatorname{vec}(\operatorname{vec}(\hat{M}_{(0,0,\cdots,0,0)})^{\dagger} \operatorname{vec}(\hat{\rho}_{(0,0,\cdots,0,1)}))^{\dagger} \\ \operatorname{vec}(\operatorname{vec}(\hat{M}_{(0,0,\cdots,0,1)})^{\dagger} \operatorname{vec}(\hat{\rho}_{(0,0,\cdots,0,1)}))^{\dagger} \\ \vdots \\ \vdots \end{bmatrix}, (18)$$

where the input states $\hat{\rho}_{(i,j,\cdots)}$ are given by

$$\hat{\rho}_{(i,j,\cdots)} = \hat{U}_i |0\rangle\langle 0|\hat{U}_i^{\dagger} \otimes \hat{U}_j |0\rangle\langle 0|\hat{U}_j^{\dagger} \otimes \cdots .$$
 (19)

TOMOGRAPHY OF ENTANGLED STATES AND PROCESSES

Given this machinery we can apply it to verfying the correlations in entangled states and reconstructing processes that create entanglement. We use an echoed cross-resonance interaction as an entangling two-qubit gate [29]. The single-qubit pulses used were 40 ns long and the total duration of the refocused $ZX_{-\pi/2}$ was 370 ns.

Despite our imperfect single-shot readout we clearly witness high-fidelity entanglement. The shot-by-shot correlation approach allows us to see correlations that are not present in the product of the averages. In Fig. 4(a) the product state shows a large response in the individual measurements and two-qubit terms that are simply the product of the single-qubit terms. Whereas in Fig. 4(b and c), we have an elegant demonstration of how maximally entangled states have only correlated information: for the single-qubit operators, in all readouts we observe a zero-mean response; however, certain two-qubit terms show maximal response.

Process tomography, shown in Fig. 5, follows in a similar fashion. Applying the procedure outlined above we find a gate fidelity for the $ZX_{-\pi/2}$ gate of 0.88. This process map clearly demonstrates that our two-qubit interaction works on arbitrary input states, and that the single-shot correlation strategy can recover information in arbitrary two-qubit components in the resulting states.

CONCLUSION

Systems such as circuit QED with continuous measurment outcomes provide a choice of strategies for qubit measurements. We show that is is possible, and sometimes preferrable, to directly correlate the continuous values without thresholding. This is an important tool when high-fidelity readout is not available on all channels. We

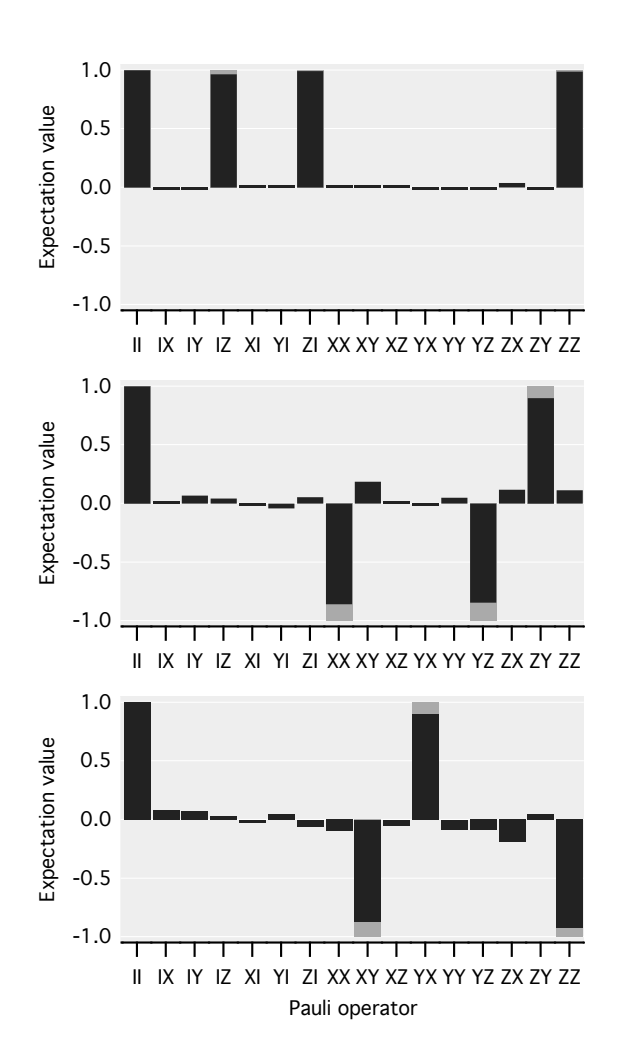


FIG. 4. Measured (black) and ideal (grey) Pauli decompositions of three two qubit states showing both product and entangled states. From top to bottom: the thermal ground state $|00\rangle$; the entangled state after applying the $\mathrm{ZX}_{-\pi/2}$ gate to a $(I-Y)\otimes (I+Z)$ input state; the entangled state after applying $\mathrm{ZX}_{-\pi/2}$ to a $(I-X)\otimes (I+Y)$ input. The fidelities, $F=\langle\psi|\rho|\psi\rangle$, of the entangled states to the ideal states $|\psi\rangle$ are 0.90 and 0.92, respectively. The product state (top) is highlighted by the presence of weight-one terms, whereas in the entangled states these terms are nearly zero.

further have provided a straightforward protocol to experimentally derive a nearly optimal linear filter to handle the transient response of a pulsed measurement. Building on this we have constructed multi-qubit measurement operators from shot-by-shot correlation of single-qubit measurement records. The SNR of these correlated operators decreases exponentially with the number of qubits, but in the high SNR regime multibody correlations of a handful of qubits are still accessible. This provides a framework for verifying quantum operations in architectures with imperfect single-qubit measurements.

The authors would like to thank George A. Keefe and Mary B. Rothwell for device fabrication. This research

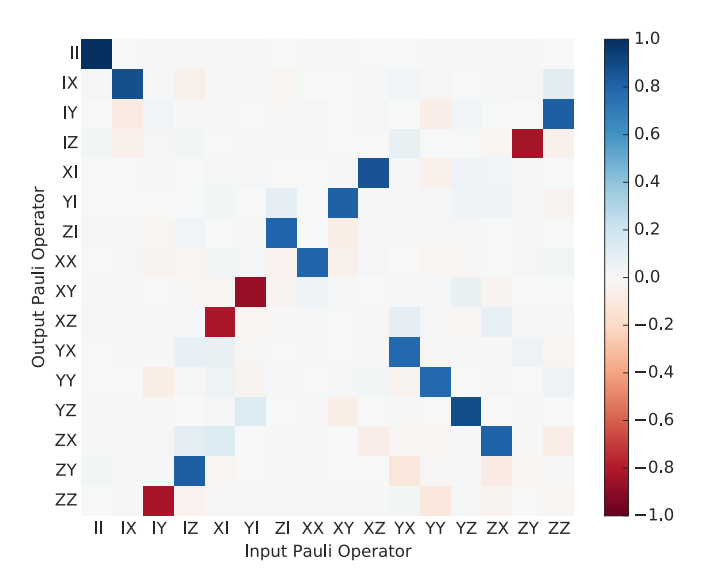


FIG. 5. Pauli transfer matrix of a $ZX_{-\pi/2}$ gate measured with correlated readouts.

was funded by the Office of the Director of National Intelligence (ODNI), Intelligence Advanced Research Projects Activity (IARPA), through the Army Research Office contract no. W911NF-10-1-0324. All statements of fact, opinion or conclusions contained herein are those of the authors and should not be construed as representing the official views or policies of IARPA, the ODNI, or the U.S. Government.

- R. Jozsa and N. Linden, Proceedings of the Royal Society A: Mathematical, Physical and Engineering Sciences 459, 2011 (2003).
- [2] J. M. Chow, L. DiCarlo, J. M. Gambetta, A. Nunnenkamp, L. S. Bishop, L. Frunzio, M. H. Devoret, S. M. Girvin, and R. J. Schoelkopf, Physical Review A 81, 062325 (2010).
- [3] S. Filipp, P. Maurer, P. Leek, M. Baur, R. Bianchetti, J. Fink, M. Göppl, L. Steffen, J. Gambetta, A. Blais, and A. Wallraff, Physical Review Letters 102, 200402 (2009).
- [4] D. Leibfried, E. Knill, S. Seidelin, J. Britton, R. B. Blakestad, J. Chiaverini, D. B. Hume, W. M. Itano, J. D. Jost, C. Langer, R. Ozeri, R. Reichle, and D. J. Wineland, Nature 438, 639 (2005).
- [5] Y.-x. Liu, L. Wei, and F. Nori, Physical Review B 72, 014547 (2005).
- [6] R. McDermott, R. W. Simmonds, M. Steffen, K. B. Cooper, K. Cicak, K. D. Osborn, S. Oh, D. P. Pappas, and J. M. Martinis, Science (New York, N.Y.) 307, 1299 (2005).
- [7] K. C. Nowack, M. Shafiei, M. Laforest, G. E. D. K. Prawiroatmodjo, L. R. Schreiber, C. Reichl, W. Wegscheider, and L. M. K. Vandersypen, Science 333, 1269 (2011).
- [8] J. B. Altepeter, D. F. James, and P. G. Kwiat, in *Quantum State Estimation*, Lecture Notes in Physics, Vol. 649, edited by M. Paris and J. Reháček (Springer Berlin Heidelberg, Berlin, Heidelberg, 2004).

- [9] D. Bozyigit, C. Lang, L. Steffen, J. M. Fink, C. Eichler, M. Baur, R. Bianchetti, P. J. Leek, S. Filipp, M. P. da Silva, A. Blais, and A. Wallraff, Nature Physics 7, 154 (2010).
- [10] C. Eichler, C. Lang, J. M. Fink, J. Govenius, S. Filipp, and A. Wallraff, Physical Review Letters 109, 240501 (2012).
- [11] A. Wallraff, D. Schuster, A. Blais, L. Frunzio, J. Majer, M. Devoret, S. Girvin, and R. Schoelkopf, Physical Review Letters 95, 060501 (2005).
- [12] D. P. DiVincenzo, Physica Scripta T137, 014020 (2009).
- [13] In both cases this can lead to systematic errors if coherent imperfections are present, e.g. wrong basis from rotation errors. Full measurement tomography, with perfect state preparation, could correct for these more general biases. Or, in the case of soft-averaging access to a calibration that is state-preparation independent could also side-step this issue.
- [14] M. A. Castellanos-Beltran, K. D. Irwin, G. C. Hilton, L. R. Vale, and K. W. Lehnert, Nature Physics 4, 929 (2008).
- [15] N. Bergeal, F. Schackert, M. Metcalfe, R. Vijay, V. E. Manucharyan, L. Frunzio, D. E. Prober, R. J. Schoelkopf, S. M. Girvin, and M. H. Devoret, Nature 465, 64 (2010).
- [16] M. Hatridge, R. Vijay, D. H. Slichter, J. Clarke, and I. Siddiqi, Physical Review B 83, 134501 (2011).
- [17] M. P. da Silva, D. Bozyigit, A. Wallraff, and A. Blais, Physical Review A 82, 043804 (2010).
- [18] L. A. Goodman, Journal of the American Statistical Association 57, 54 (1962).
- [19] J. M. Chow, J. M. Gambetta, a. D. Córcoles, S. T. Merkel, J. a. Smolin, C. Rigetti, S. Poletto, G. a. Keefe, M. B. Rothwell, J. R. Rozen, M. B. Ketchen, and M. Steffen, Physical Review Letters 109, 060501 (2012).
- [20] A. Blais, R.-S. Huang, A. Wallraff, S. Girvin, and R. Schoelkopf, Physical Review A 69, 062320 (2004).
- [21] M. Jerger, S. Poletto, P. Macha, U. Hubner, E. Ilichev, and a. V. Ustinov, Applied Physics Letters 101, 042604 (2012).
- [22] S. McHugh, B. A. Mazin, B. Serfass, S. Meeker, K. O'Brien, R. Duan, R. Raffanti, and D. Werthimer, Review of Scientific Instruments 83, 044702 (2012).
- [23] J. Gambetta, W. Braff, A. Wallraff, S. Girvin, and R. Schoelkopf, Physical Review A 76, 012325 (2007).
- [24] J. Gambetta, A. Blais, M. Boissonneault, A. Houck, D. Schuster, and S. Girvin, Physical Review A 77, 012112 (2008).
- [25] G. Turin, IEEE Transactions on Information Theory 6, 311 (1960).
- [26] E. Magesan, J. M. Gambetta, and J. Emerson, Physical Review Letters 106, 180504 (2011).
- [27] R. Kosut, I. A. Walmsley, and H. Rabitz, arXiv preprint (2004), quant-ph/0411093.
- [28] K. Blum, Density Matrix Theory and Applications, Springer Series on Atomic, Optical, and Plasma Physics, Vol. 64 (Springer Berlin Heidelberg, Berlin, Heidelberg, 2012).
- [29] A. D. Córcoles, J. M. Gambetta, J. M. Chow, J. a. Smolin, M. Ware, J. Strand, B. L. T. Plourde, and M. Steffen, Physical Review A 87, 030301 (2013).